environments

MDPI

Article

Use of Water Balance and Tracer-Based Approaches to Monitor Groundwater Recharge in the Hyper-Arid Gobi Desert of Northwestern China

Tomohiro Akiyama [1,*], Jumpei Kubota [2], Koji Fujita [3], Maki Tsujimura [4], Masayoshi Nakawo [2], Ram Avtar [5] and Ali Kharrazi [6,7,*]

1 Department of Socio-Cultural Environmental Studies, Graduate School of Frontier Sciences, the University of Tokyo, Kashiwa 277-8563, Japan
2 Research Institute for Humanity and Nature, Kyoto 603-8047, Japan; jkubota@chikyu.ac.jp (J.K.); nakawom@gmail.com (M.N.)
3 Graduate School of Environmental Studies, Nagoya University, Nagoya 464-8601, Japan; cozy@nagoya-u.jp
4 Faculty of Life and Environmental Sciences, University of Tsukuba, Tsukuba 305-8577, Japan; mktsuji@geoenv.tsukuba.ac.jp
5 Graduate School of Environmental Earth Science, Hokkaido University, Sapporo 060-0810, Japan; ram.envjnu@gmail.com
6 Advanced Systems Analysis Group, International Institute for Applied Systems Analysis (IIASA), Laxenburg A-2361, Austria
7 Center for the Development of Global Leadership Education, the University of Tokyo, Tokyo 113-8654, Japan
* Correspondence: akiyama@k.u-tokyo.ac.jp (T.A.); kharrazi@iiasa.ac.at (A.K.); Tel.: +81-04-7136-4814 (T.A.)

Received: 20 April 2018; Accepted: 30 April 2018; Published: 4 May 2018

Abstract: The groundwater recharge mechanism in the hyper-arid Gobi Desert of Northwestern China was analyzed using water balance and tracer-based approaches. Investigations of evaporation, soil water content, and their relationships with individual rainfall events were conducted from April to August of 2004. Water sampling of rainwater, groundwater, and surface water was also conducted. During this period, 10 precipitation events with a total amount of 41.5 mm, including a maximum of 28.9 mm, were observed. Evaporation during the period was estimated to be 33.1 mm. Only the soil water, which was derived from the heaviest precipitation, remained in the vadose zone. This is because a dry surface layer, which was formed several days after the heaviest precipitation event, prevented evaporation. Prior to that, the heaviest precipitation rapidly infiltrated without being affected by evaporation. This is corroborated by the isotopic evidence that both the heaviest precipitation and the groundwater retained no trace of significant kinetic evaporation. Estimated δ-values of the remaining soil water based on isotopic fractionation and its mass balance theories also demonstrated no trace of kinetic fractionation in the infiltration process. Moreover, stable isotopic compositions of the heaviest precipitation and the groundwater were very similar. Therefore, we concluded that the high-intensity precipitation, which rapidly infiltrated without any trace of evaporation, was the main source of the groundwater.

Keywords: groundwater recharge; evaporation; water balance; stable isotopes; hyper-arid environment; Gobi Desert; Northwestern China

1. Introduction

Groundwater is the most important water resource for people living in hyper-arid deserts where the ratio of mean annual precipitation to mean annual potential evapotranspiration is less than 0.05 [1]. Nevertheless, new exploitation of groundwater resources has also been rapidly developing in the Gobi Desert of Northwestern China without an understanding of its groundwater recharge mechanism.

Recent studies conducted under more humid conditions, such as those in semi-arid and arid areas, indicated that a significant recharge might occur even where annual potential evapotranspiration significantly exceeds precipitation [2–5]. The groundwater recharge rates of these studies ranged from 1 to 30% of the local precipitation [6,7]. Considerable soil water, augmented by precipitation, recharged the groundwater being affected by evaporation [5,8,9]. Thus, the resulting stable isotopic composition of the groundwater, in comparison to the source water in nearby areas, was depleted [5,10–12]. In recent studies, researchers also noticed that land use/land cover has an impact on groundwater recharge [13]. In hyper-arid areas, however, it is not well understood whether precipitation might induce groundwater recharge since measurements of groundwater recharge in hyper-arid areas are extremely difficult [3].

The main techniques used to understand the groundwater recharge mechanism can be divided into physical methods such as water balance and lysimeter measurement, and chemical methods such as tracer techniques [8,14–18]. However, estimations of recharge, by whatever method, are subject to major uncertainties and errors [19]. Given the uncertainties associated with each individual approach, multiple techniques should be used to study groundwater recharge processes [20].

The objectives of this study are to analyze groundwater recharge mechanisms in a hyper-arid environment using water balance and tracer-based approaches. Investigations of evaporation, soil water content, and their relationships with individual rainfall events were conducted in the Gobi Desert which is located in the lower reaches of the Heihe River basin. Evaporation, which was estimated using the Penman-Monteith equation, with additional considerations of water vapor transport from soil pores in the soil surface layer to the atmosphere, was cross-checked by two independent estimations. These independent estimations included the eddy correlation method and the weighing lysimeter. Stable isotopic fractionation and its mass balance theories were used to understand the effect of evaporation on stable isotopes in discussing the relationship between precipitation and groundwater. In this study, we used physical methods and tracer techniques to improve our understanding of groundwater processes.

2. Study Area

2.1. Hydrogeological and Lithological Settings

The Heihe River basin is the second largest inland river basin in China. The river is 821 km long with a watershed area of 130,000 km^2. There are three geological units in the basin; these are respectively, the Qilian Paleozoic geosynclinals fold zone, the Hexi Corridor depression, and the northern fault-block uplift [21]. The uplift of the Qilian geosyncline occurred from the end of the Palaeozoic throughout the whole Mesozoic era and created the embryonic form of the Hexi Corridor. This was followed by a complex tectonic stage when the Longshoushan-Helishan structural zone was formed in the Hexi Corridor.

Following the geological characteristics, the basin can be divided into three reaches. As illustrated in Figure 1, these include the upper mountainous, middle oasis, and lower desert reaches. The upper reaches are the Qilian Mountains with a glacier area of 73 km^2 which cover 0.7% of the reaches [22]. The middle and lower reaches are separated by the Longshoushan-Helishan Mountains. The middle reaches are composed of the piedmont alluvial fan and a fine earthy plain. The irrigated agricultural farmland is mainly located in the fine earthy plain [23]. The lower reaches are an alluvial and lacustrine plain underlaid with unconsolidated sediments from the Quaternary age. The topography of the lower reaches inclines from the southwest to the northeast with an average slope of 1–3%. The Quaternary alluvium, consisting of fluviatile sand, gravel, and silt to a depth of several hundred meters, is widely distributed in the lower reaches [24,25]. The lithologic characters of the aquifer system gradually vary from gravel to fine sand, from the south to the north of the lower reaches [21].

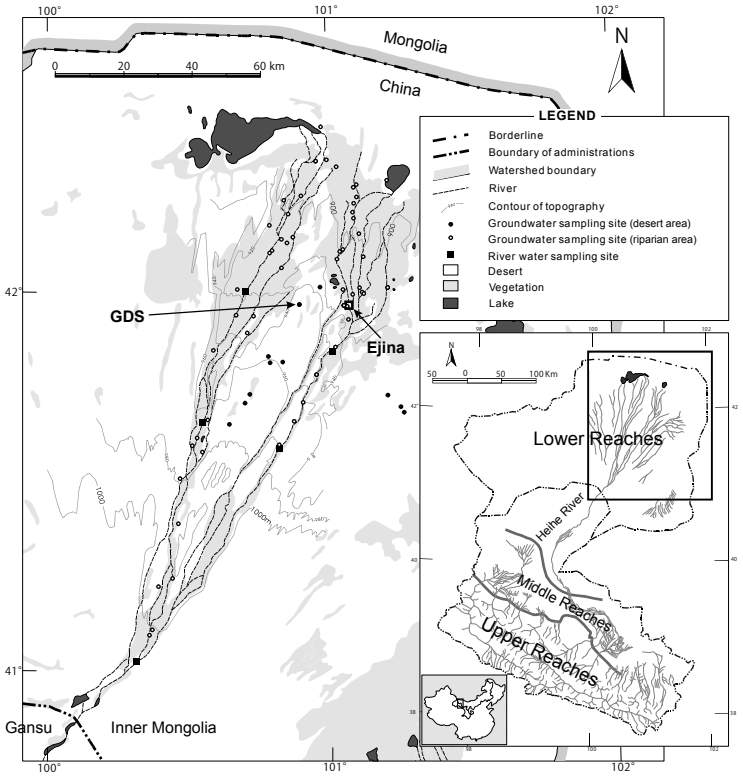

Figure 1. Map of study area. Gobi Desert site (GDS) indicates study site. Vegetation classification was based on Grassland type map of Heihe River basin, China [26].

The annual ranges of precipitation in the upper, middle, and lower reaches are respectively, 300 mm to 500 mm, 100 mm to 300 mm, and less than 100 mm [27]. More than 90% of the precipitation in all the reaches occurs from April to September. Annual precipitation observed at Ejina (Figure 1) was 38.4 mm on average, with a range from 13.4 mm to 103.3 mm from 1950 to 2000. Annual pan evaporation was 3489 mm on average, with a range of 2987 mm to 4384 mm during the same period. While there is riparian vegetation along the Heihe River, due to the hyper-arid condition, the lower reaches consist of large expanses of gravel desert called the Gobi Desert.

2.2. Groundwater Recharge Sources in the Heihe River Basin

Groundwater recharge in the Heihe River basin is different because of the difference in landform units. Previously, researchers have suggested the use of base-flow separation and water-balance methods respectively, in the upper and middle reaches, to determine the quantity of groundwater recharge [28]. Furthermore, previous research has revealed average groundwater recharge in the middle reaches to be ~20.8 $\times$ 10^8 m^3 a^{-1} from 1990 to 1995 [29]. Of this total, 4.3 $\times$ 10^8 m^3 a^{-1} were contributed by precipitation, groundwater inflows, and infiltration of mountain-front surface runoff; 6.1 $\times$ 10^8 m^3 were contributed by leakage from river and stream channels; 8.7 $\times$ 10^8 m^3 by leakage from artificial channels; and 1.7 $\times$ 10^8 m^3 by infiltration on irrigated farmland [29].

Our study site, the Gobi Desert Site (GDS), is located in the lower reaches of the Hehe River Basin (Figure 1). Possible groundwater recharge sources in the study site include river infiltration and diffuse/direct recharge from precipitation. The possibility of lateral groundwater flow is excluded because the lateral groundwater flow from the middle reaches was almost entirely transformed into surface water due to an effect of piedmont tectonic barriers at the boundary between the middle and the lower reaches [27]. Generally, researchers think the Heihe River is the main source of groundwater recharge in the lower reaches. The presence of a wide and shallow riverbed and phreatic aquifer, which consists of coarse sand and gravel with a high permeability, means high groundwater

recharge [30]. Approximately 68% of the seasonal river water seeps into recharging groundwater and groundwater flows from the southwest to the northeast across the basin. The groundwater table inclines from the southwest to the northeast with an average slope of about 1%. In the meantime, Akiyama et al. studied the daily dynamics of groundwater level, that is, the distance from groundwater table to ground surface, in the desert area of the lower reaches and noticed that the annual changes in groundwater level, reaching 0.10 m, may be affected by direct rainfall recharge [31] (DE site in Figure 3a of [31] corresponds to GDS site in the present study.). The groundwater level in the desert area of the lower reaches ranged from 1.12 m to 2.88 m with an average of 1.5 m. Shortage of water can lead towards a serious problem in the watershed; therefore, the study of various sources of groundwater recharge in this region is of critical importance for agricultural and environmental public policy.

3. Methods

3.1. Water Balance Approach

3.1.1. Hydrological and Meteorological Observations

Hydrological and meteorological observations and data collections were made at the Gobi Desert Site (GDS) (Figure 1) from 28 April until 28 August 2004. Two types of observations were made to measure precipitation; one was a simple visual observation using funnel and plastic bottle; the other was an automatic observation using a tipping bucket with a logger (HoBo-event, Onset) whose resolution was 0.1 mm. In addition, the wetting front after the heaviest precipitation event was visually observed at several trenches.

An eddy correlation system was installed to measure turbulent fluxes at the same site. The eddy correlation method is an established method to accurately estimate evapotranspiration based on measurements of turbulent fluxes. We used the method to estimate evapotranspiration for the validation of data. A 3-dimensional sonic anemometer (CYG-81000, R. M. YOUNG, Traverse, MI, USA) was used to measure the fluctuations in wind velocity components and temperatures. An open-path infrared gas analyzer (LI-7500, Licor, Lincoln, NE, USA) was employed to measure the concentrations of water vapor. These measurements were made at 10 Hz on a CR5000 data logger (Campbell Scientific, Ltd., Loughborough, UK). The fluxes were later calculated off-line after performing coordinated rotations, correcting the sonic temperature for the lateral velocity and presence of humidity, making frequency response corrections for slow apparatus and path length integration, and the inclusion of the mean vertical velocity according to [32].

An Automatic Weather Station (AWS) including the Time Domain Reflectometry (TDR) system and a weighing lysimeter (0.20 m in diameter) system was also installed to model evapotranspiration. Measurements of net radiation, incoming and outgoing short-wave and long-wave radiations, air temperature, relative humidity, wind speed and direction, soil moisture, soil temperature, and soil heat flux, soil water storage in the lysimeter were recorded as average values at 10-min intervals on a CR-10X data logger (Campbell Scientific, Ltd.). TDR sensors (CS615, Campbell Scientific, Ltd.) were installed at depths of 0.05 m, 0.10 m, 0.30 m, and 0.70 m. Ground temperature sensors were installed at depths of 0 m, 0.02 m, 0.05 m, and 0.10 m, and used to calibrate TDR data according to [33]. Evaporation was estimated by substituting this meteorological dataset into the following Penman-Monteith equation revised with additional consideration of water vapor transport from soil pores in the soil surface layer to the atmosphere.

3.1.2. Penman-Monteith Equation

The Penman-Monteith equation [34] is useful for computing evaporation rates of bare soil. However, this equation becomes less useful for evaluation of water vapor transport from soil pores in the dry soil surface layer to the atmosphere. Kondo et al. [35] used the vapor diffusion distance $F(\theta)$ (m) representing resistance to water vapor diffusion from the interior of the soil pores to the land

surface. Kondo et al. [35] and Saigusa [36] demonstrated that $F(\theta)$ is well defined as a function of the soil water content θ as

$$F(\theta) = F_1(\theta_{sat} - \theta)^{F_2} \quad (1)$$

where F_1 and F_2 are respective parameters dependent on soil types, and θ_{sat} is the saturation soil water content. These parameters were determined experimentally.

We applied them together with the Penman-Monteith equation to estimate the latent heat flux, ιE as

$$\iota E = \frac{\Delta(Rn - G) + \rho C_p[q^*(T_s) - q]/r_a}{\Delta + \gamma(1 + r_s/r_a)} \quad (2)$$

$$\Delta = \frac{q^*(T_s) - q^*(T_a)}{T_s - T_a} \quad (3)$$

$$r_s = {}^{F(\theta)}/_{D_{atm}} \quad (4)$$

$$r_a = {}^{1}/_{C_H u} \quad (5)$$

where Rn is the net radiation, and G is the heat flux into the ground. ι is the latent heat at a unit mass of water. T_a, q and u are the ground-level (at a height of approximately 1 m) air temperature, specific humidity, and wind speed, respectively. $q^*(T_s)$ is the saturated specific humidity at the surface temperature T_s. c_p and ρ are specific heat of air at a constant pressure and the air density, respectively. γ is the psychrometer constant, r_s the surface resistance, r_a the aero dynamic resistance, C_H the bulk coefficient, and D_{atm} is the molecular diffusivity of water vapor.

In a way similar to [37], bulk coefficient was parameterized dependent on the atmospheric stability R_{ib} as

$$C_H = exp(-5.5 - 15.0R_{ib}) + 0.0012 \quad (6)$$

for stable conditions ($R_{ib} > 0$), while

$$C_H = 0.0415 \exp(-29.416\theta),\ \theta \leq 0.083 \quad (7)$$

$$C_H = 0.0037,\ \theta \leq 0.083 \quad (8)$$

for unstable conditions ($R_{ib} \leq 0$). The R_{ib} is defined as

$$R_{ib} = \frac{g}{T_m} \times \frac{z(T_s - T_a)}{u^2} \quad (9)$$

where T_m is the average between T_s and T_a, and z the observation height of both T_a and u [38].

3.2. Tracer-Based Approach

We conducted water sampling of shallow groundwater, river water, precipitation, and water vapor within the lower desert reaches. Shallow groundwater was collected at 56 sites (Figure 1) in desert and riparian vegetated areas to understand spatial differences in isotopic composition in February and June of 2002, and September and October of 2003. At the same time, river water was also collected. Precipitation in various amounts and intensities was collected using a funnel and a plastic bottle with paraffin oil to prevent evaporation from the rainwater samples from June 2002 to August 2004. Water vapor in ambient air was collected with an electric dehumidifier during 30 min of each sampling from April to August in 2004. All samples were filtrated by using 0.20-μm filters before sealing in polyethylene bottles.

The stable isotopic composition was analyzed for all samples using a water equilibration system coupled to a mass spectrometer (ThermoQuest DeltaPlus, Austin, TX, USA) maintained by the Hydrospheric Atmospheric Research Center (HyARC), Nagoya University, Japan. The isotopic ratios

of water, $^{2}H/^{1}H$ and $^{18}O/^{16}O$, are expressed in terms of permill deviations from those of Standard Mean Ocean Water (SMOW),

$$\delta = \left(R_{sample}/R_{smow} - 1\right) \times 10^{3} \quad (10)$$

where R is the isotopic ratio $^{2}H/^{1}H$ or $^{18}O/^{16}O$. Reproducibility was 0.03‰ and 0.5‰ for $\delta^{18}O$ and δD, respectively. These stable isotopes of water are beneficial to study hydrological cycles, ecological processes, and paleoclimates [39].

Deuterium excess (often shortened to "d-excess") varied as a result of kinetic fractionation is also used as a tracer [8,40,41].

$$d = \delta D - 8\delta^{18}O \quad (11)$$

This value is the δD intercept value of a line with a slope of 8 fitted through a dataset, and typically has values close to +10‰ for rain samples in temperate climates. The d-excess in arid groundwater has been observed to be in the order of +5 to +6 [10,11]. There are two possible causes for these low d-excesses: (1) its source water evaporated in the recharge process, which may cause the evaporative enrichment of residual water [8], and (2) meteoric water that initially evaporated from the ocean under more humid conditions than those at present [42].

Mass balances in the groundwater recharge processes can be represented, in the absence of significant surface runoff, by the follows equations:

$$R \times \delta_R = P \times \delta_P - E \times \delta_E - \Delta S \times \delta_S \quad (12)$$

$$R = P - E - \Delta S \quad (13)$$

where R is groundwater recharge, P is precipitation, E is evaporation, and ΔS is change in soil water storage in a vadose zone. All components are given as rates (e.g., mm day^{-1} or mm a^{-1}). δ_R, δ_P, δ_E, and δ_S represent δ-values respectively of recharging water, precipitation, evaporating water vapor, and soil water. Under the assumption that water surface and atmospheric temperatures are the same, [43] simplified δ_E, which was first defined by [44] as

$$\frac{\delta_E}{10^3} + 1 = \frac{\alpha_k}{1-h} \times \left[\alpha \times \left(\frac{\delta_L}{10^3} + 1\right) - h \times \left(\frac{\delta_a}{10^3} + 1\right)\right] \quad (14)$$

where δ_E, δ_L, and δ_a stand for δ-values of evaporating water vapor, a liquid water body, and ambient air, respectively, α and α_k are the equilibrium and kinetic fractionation factors, and h is the relative humidity $(0 \leq h \leq 1)$. Majoube [45] expressed the equilibrium fractionation factor as a function of water surface temperature T (K):

$$\ln(1/\alpha) = 1.137 \times 10^{3}/T^{2} - 0.4156/T - 2.0667 \times 10^{-3} \text{ for } ^{18}\text{O}. \quad (15)$$

$$\ln(1/\alpha) = 24.844 \times 10^{3}/T^{2} - 76.248/T + 52.612 \times 10^{-3} \text{ for D}. \quad (16)$$

α_k ranges 1.015–1.031 and 1.013–1.026 respectively for δ^{18}O and δD, with high values for diffusive boundary layers and low values for turbulent boundary layers [46–49]. Suppose R is zero, δ-values of the soil water are provided as

$$\delta_s = \frac{\delta_P - f \times \delta_E}{1 - f} \quad (17)$$

where f is the fraction of evaporation against precipitation.

4. Data

4.1. Precipitation

Figure 2a shows the daily precipitation observed at the Gobi Desert Site from May to August in 2004. Precipitation events were observed a total of 10 times. The maximum precipitation was 28.9 mm

on 3 June (Julian day of the year (DOY) 155). On the following two days, precipitation occurred intermittently. The total amount of precipitation during the observation period was 41.5 mm.

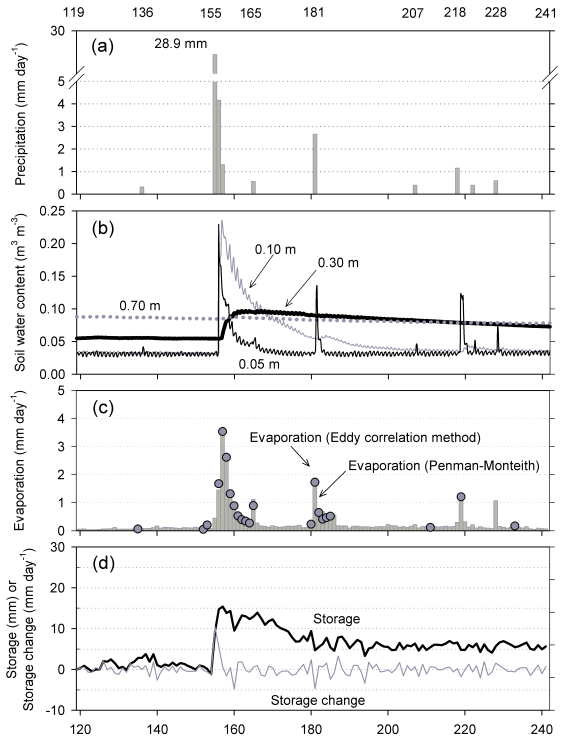

Figure 2. (**a**) Time series for daily precipitation at Gobi Desert site. Julian days indicating precipitation events were shown on the top horizontal axis. (**b**) Time series for volumetric soil water content at depths of 0.05 m, 0.10 m, 0.30 m, and 0.70 m. (**c**) Time series for daily evaporation independently estimated by using the present model based on the Penmman-Monteith equation (bar) and eddy correlation method (dot). (**d**) Time series for daily mean water storage in lysimeter and its storage change.

4.2. Soil Water Content and Wetting Front and Their Responses to Precipitation

Figure 2b shows soil water content at the Gobi Desert site. At the beginning of the observation, the soil water content at a depth of 0.05 m was 0.03, showing a completely dry condition. The soil water content at a depth of 0.05 m increased after every precipitation event. The soil water content at a depth of 0.10 m increased after only three events with a precipitation amount of more than 1.0 mm on 3 June (DOY 155), 29 June (DOY 181) and 5 August (DOY 218). The soil water content at a depth of 0.30 m increased only after the heaviest precipitation on 3 June (DOY 155). Little significant change was found at a depth of 0.70 m during the observation. These results suggest that heavy precipitation induced an infiltration level deeper than 0.30 m.

Moreover, the infiltration induced due to the heaviest precipitation was rapid. Only 1 day after the event, the soil water content at a depth of 0.30 m started to increase (Figure 2b). Similar results showing rapid infiltration after the heaviest precipitation were obtained from the observation of the wetting front shown in Figure 3. The wetting front at 12 h after the precipitation had already reached about 0.16 m. The wetting front reached 0.23 m at 45 h, and 0.38 m at 93 h. The infiltration rate over the first 12 h was 0.33 m day^{-1}. While we confirmed groundwater level started to rise due to the diffuse recharge, it became difficult to determine the wetting front since 96 h had passed after the heaviest precipitation [31]. (Groundwater level data during the observation period is available in Figure 3a of [31]. DE site in the figure corresponds to GDS site in the present study.).

Next, the patterns of decrease in soil water content after each precipitation event are shown in Figure 2b. The soil water content at depths of 0.05 m and 0.10 m reached the dry condition

immediately after each precipitation event, whereas the soil water content at 0.30 m never reverted to the pre-precipitation condition, even 80 days after the heaviest precipitation. This is evidence that the soil water remained in the vadose zone without being affected by evaporation. The water content at the depth of 0.7 m was significantly higher than the soil zone above the 0.7 m depth—this could be due to the capillary fringe.

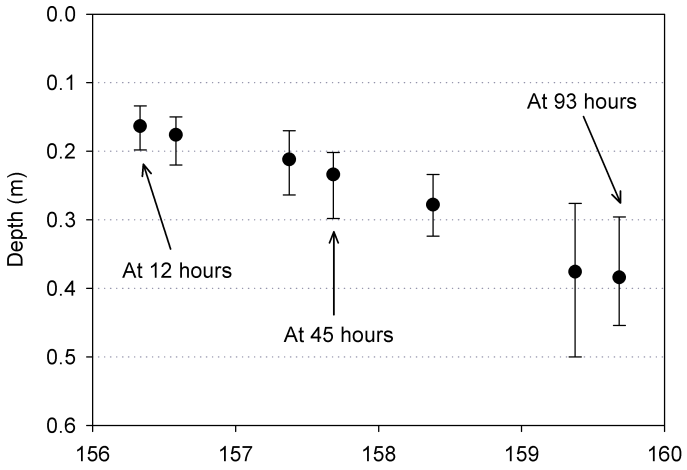

Figure 3. Wetting front observed after heaviest precipitation on 3 June (DOY 155) at Gobi Desert site. Bars are standard deviations (n = 14).

5. Results

5.1. Results of Water Balance Approach

5.1.1. Energy Balance and Its Relation to Soil Water Content near the Surface

Turbulent fluxes at the Gobi Desert site were estimated using the eddy correlation method. Figure 4a shows hourly changes in the energy balance after the precipitation event on DOY 181 (2.7 mm) with prevailing dry conditions on 30 and 31 May (DOY 151 and 152). Maximum latent heat flux was observed as 167 Wm^{-2} at 9 A.M. local time on DOY 181, and turned to decrease at a rate of 30 Wm^{-2} every hour. In association with the decrease in the latent heat flux, the sensible heat flux increased. Hourly changes in the surface resistance and soil water content at a depth of 0.05 m after the heaviest precipitation are shown in Figure 4b. The soil water content showed a sudden drop to about 0.03. In association with the decrease, the surface resistance significantly increased as high as the one under dry conditions. These results can be attributed to the fact that the small amount of precipitation completely evaporated immediately. Evaporation the following two days after the precipitation event was estimated as 2.6 mm, which was nearly the same as the precipitation amount.

Figure 4a also shows hourly changes in the energy balance after the heaviest precipitation events from DOY 155 to DOY 157 (34.4 mm). Maximum latent heat flux was observed to be about 300 Wm^{-2} at 0 P.M. local time on DOY 157. Daily mean latent heat flux gradually decreased and became less than 10 Wm^{-2} eight days later (DOY 163). Evaporation during the experiment was estimated to be 12.5 mm, which was about one-third of the precipitation amount. The surface resistance increased due to a decrease in the soil water content and reached a high level on DOY 163 similar to that under previous dry conditions. These results indicated that a dry surface layer which formed several days later prevented evaporation from water stored in the soil.

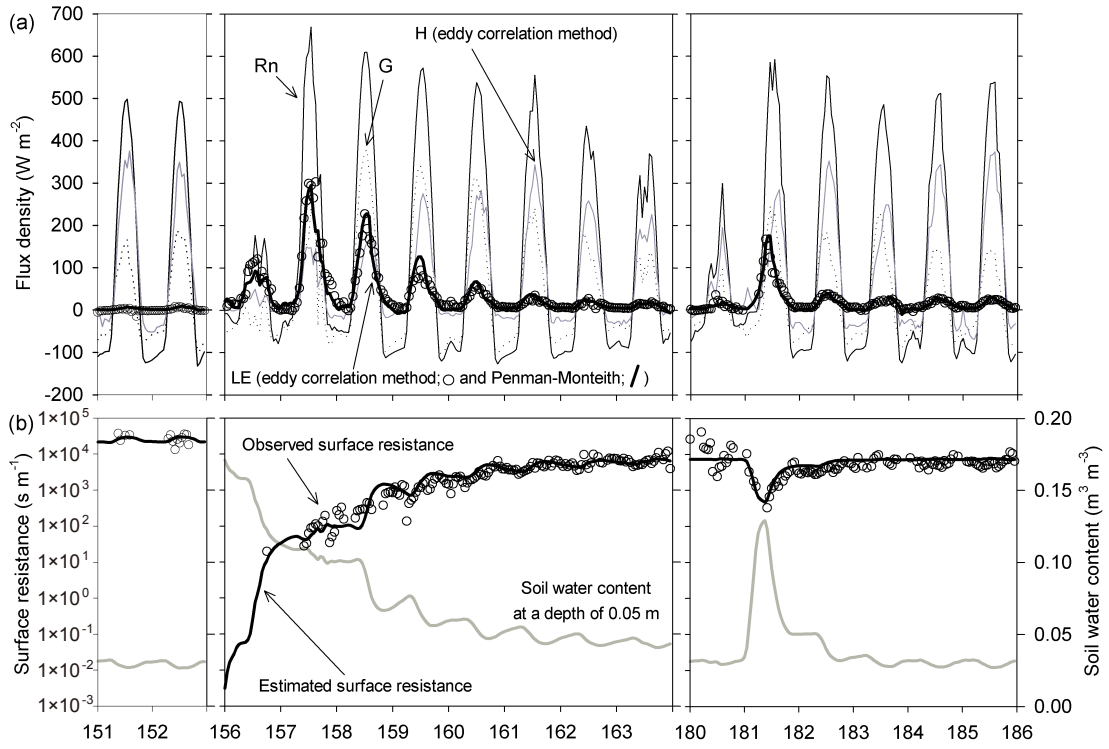

Figure 4. Time-series for hourly net all-wave radiation, ground heat flux, latent heat flux, and sensible heat flux (**a**), surface resistance and volumetric soil water content at 0.05 m depth (**b**) after heaviest precipitation on 3 June (DOY 155) of 28.9 mm, and lighter precipitation on 29 June (DOY 181) of 2.7 mm at Gobi Desert site.

5.1.2. Water Balance

Latent heat flux was also calculated using Equation (2) with the function $F(\theta)$ in Equation (1) and the parameterized bulk coefficients in Equations (6)–(8). Sensible heat flux was obtained as a residual of observed net radiation, ground heat flux, and estimated latent heat flux. Figure 4a includes latent heat flux estimated using the Penman-Monteith equation. The figures show general agreement between latent heat fluxes estimated by the Penman-Monteith equation and the eddy correlation method. The root mean square error (RMSE) for 618 h of data was 11 Wm^{-2} and 33 Wm^{-2} for the latent heat and sensible heat fluxes, respectively.

Based on hourly calculations of the latent heat flux, we determined the daily evaporation. Figure 2c depicts daily evaporation obtained by both the Penman-Monteith equation and the eddy correlation method, and shows good agreement between them, with its RMSE being 0.1 mm day^{-1} for 23 days of data. The calculated evaporation using the Penman-Monteith equation and observed precipitation was 33.1 mm and 41.5 mm, respectively (involving the heaviest precipitation, 28.9 mm), during the observation period. Water totaling 8.4 mm was left in the vadose zone, which was 29% of the heaviest precipitation. This positive storage change in the vadose zone was due to nothing but the heaviest precipitation.

Figure 2d shows the daily changes in water mass storage (expressed as water depth) at the Gobi Desert site measured using a weighing lysimeter. The values of water mass storage were shown based on the initial value on 28 April (DOY 119). Unfortunately, the heaviest precipitation on 3 June (DOY 155) was not measured because it was beyond the lysimeter measuring limit. Despite the overflow, a water mass with an amount of 16.6 mm was stored in the lysimeter due to the heaviest precipitation. The increased storage gradually declined, becoming fairly constant starting on or about 18 July (DOY 200). On 28 August (DOY 241), which was the final day of the observation, a water mass in the amount of 4.9 mm remained, accounting for 30% of the input.

5.2. Results of Tracer-Based Approach

5.2.1. Stable Isotopes in Precipitation and Its Relation to Precipitation Amount

Figure 5 shows the relationship between precipitation amount and δ^{18}O and *d*-excess of each event. The δ^{18}O and *d*-excess in the precipitation showed a significantly wide variation, but clear patterns were found. Heavy precipitation was characterized as low δ^{18}O with high *d*-excess of 10, while light precipitation was characterized as high δ^{18}O with low *d*-excess.

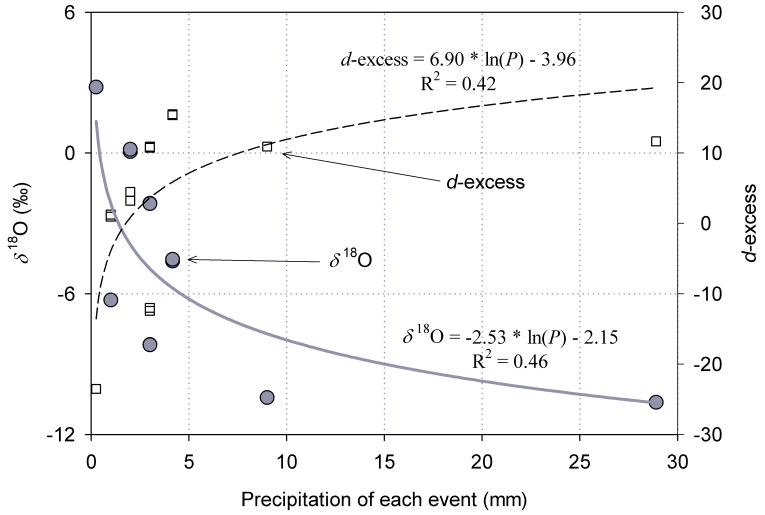

Figure 5. The relationship between precipitation amount (*P*) and δ^{18}O and *d*-excess of each precipitation event.

A δ-diagram of the precipitation is shown in Figure 6. The local meteoric water line (LMWL) was determined as

$$\delta D = 6.1\delta^{18}\mathrm{O} - 8.5 \; R^2 = 0.93 \tag{18}$$

The slope, which was lower than that of the Global Meteoric Water Line (GMWL) found by [50], suggests a significant kinetic evaporation effect in their precipitation process except for the high intensity.

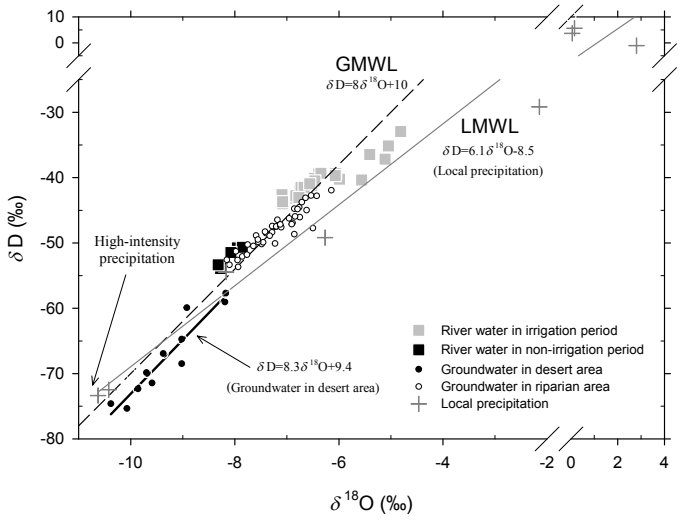

Figure 6. δ-diagram of water samples collected in lower reaches. Irrigation period indicates a period from April to September.

5.2.2. Stable Isotopes in Shallow Groundwater

A δ-diagram of groundwater collected in the lower desert reaches is also shown in Figure 6. The $\delta^{18}O$ and δD values in groundwater differed between riparian and desert areas. The δ-values were higher in the riparian areas than in the desert areas. The *t*-test demonstrated that δ-values of groundwater in the desert area were significantly different from those in the riparian area, indicating that the sources of the groundwater must be different.

The δ-diagram further shows that δ-values of the groundwater in the desert area were significantly lower than those of any river water samples. The δ-values of the groundwater were more similar to high-intensity precipitation rather than the river water. These results can be attributed to the fact that the high-intensity precipitation is one of the main sources of the groundwater.

Regression line of the groundwater in the desert area was determined as

$$\delta D = 8.3\delta^{18}O + 9.4 \; R^2 = 0.89 \quad (19)$$

The slope was more similar to that of the GMWL than that of the LMWL (Equation (18)). Therefore, the groundwater had a scarce trace of kinetic evaporation.

6. Discussion

A total of 10 precipitation events were observed at the Gobi Desert site during the observation period (Figure 2a). Only the heaviest precipitation on 3 June (DOY 155) at an amount of 28.9 mm induced a downward infiltration deeper than 0.30 m (Figures 2b and 3). The increased soil water content at the 0.30 m depth remained for more than 80 days after the precipitation (Figure 2b). In addition, the water balance analysis demonstrated that 29% of the heaviest precipitation was left in the vadose zone during the observation period (Figure 2c). This result was also supported by lysimeter observations in which 30% of the precipitation was left in the lysimeter (Figure 2d). Although there is obviously an error due to the overflow, the lysimeter results qualitatively suggested that a considerable amount of water remained in the soil. The results of both the soil water content measurement and the water balance analysis, would therefore strongly suggest the possibility of groundwater recharge due to the heaviest precipitation even in a hyper-arid environment. Indeed, we confirmed that groundwater level started to rise after the heaviest precipitation [31] (Groundwater level data during the observation period is available in Figure 3a of [31]. DE site in the figure corresponds to GDS site in the present study.).

One of the reasons why a significant amount of water remained in the vadose zone was the formation of a dry surface layer after the heaviest precipitation event. Such a dry surface layer, where water moves only in the vapor phase [51], prevents evaporation in soil due to a decrease in capillary forces (characterized by the soil moisture). The forming of a dry surface layer was indicated by decreasing the latent heat flux to less than 10 Wm^{-2} in association with both the decrease in soil water content at a depth of 0.05 m and the increase in surface resistance after the heaviest precipitation event (Figure 4).

Prior to the formation of the dry surface layer, the soil water derived from the heaviest precipitation infiltrated rapidly at a rate of 0.33 m day^{-1} (Figure 3) and remained in the vadose zone (Figure 2b). In contrast, only a small amount of precipitation completely evaporated immediately (Figures 2b and 4a). In this case, the soil water remaining in the vadose zone derived from the heaviest precipitation must have retained no trace of evaporative concentration. Moreover, if the soil water should continue to infiltrate downward and to eventually recharge the groundwater, it would also retain no trace of evaporative concentration.

This is corroborated by the isotopic evidence formed in the δ-diagram of the samples (Figure 6). Both the groundwater and the high-intensity precipitation in the desert area were plotted near the global meteoric water line, implying no significant kinetic evaporation. The δ-values of groundwater were slightly higher than those of the high-intensity precipitation. These results suggested that one of

the main sources of the groundwater was very high-intensity precipitation with no trace of a kinetic evaporation effect.

Due to difficulties of isotopic observations in the soil water, the present study cannot directly demonstrate that the soil water remaining in the vadose zone did not retain any trace of evaporative concentration. Here, we attempt to verify this by estimating δ-values of the soil water based on water and isotopic mass balances with kinetic fractionation theories. If the soil water were to have a trace of kinetic evaporation enrichment, f should be about 0.71 as calculated by the water balance analysis. If the soil water were to have no such trace of evaporation, f should be zero. Stable isotopic compositions of evaporating water vapor are calculated using Equation (14). Parameters are set as follows: 1.019 and 1.017 [47,48] for α_k (kinetic fractionation factors of δ^{18}O and δD); 283 K (annual mean air temperature) for T_a; 0.3 (annual mean relative humidity) for h_a, δ^{18}O, and δD of the high-intensity precipitation at the Gobi Desert site; with values of $-10.4‰$ and $-72.5‰$ for δ_L (δ-values of the evaporating water), δ^{18}O, and δD of water vapor; with average values of $-25.2‰$ and $-143.1‰$ observed using an electric dehumidifier at Ejina for δ_a (δ-values of the ambient air). As a result, the estimated δ^{18}O and δD of the recharging water δ_S are +55.3‰ and +177.0‰ in the case with a trace of kinetic evaporation enrichment (i.e., the fraction of evaporation against precipitation is 0.71). By contrast, without any trace of the enrichment (i.e., the fraction is zero), δ^{18}O and δD of the soil water δ_S are estimated as $-10.4‰$ and $-72.5‰$, in close agreement with annual mean δ^{18}O and δD of the groundwater observed as $-9.6‰$ and $-71.5‰$. Moreover, the d-excess for the case of a significant trace of evaporation enrichment is estimated as $-265.4‰$, while the d-excess of the soil water for the case of a significant trace of evaporation enrichment is estimated as 10.9, suggesting good agreement with the d-excess of the groundwater observed as 5.2. Therefore, it was possible that the soil water remaining in the vadose zone underwent scarcely any kinetic evaporation. In addition, the remaining soil water should undergo scarce kinetic evaporation in its recharge process due to the dry surface layer (Figure 4). We consequently conclude that nothing but high-intensity precipitation without any trace of kinetic evaporation is the main source of the groundwater in the Gobi Desert.

One notably unique difference between hyper-arid and more humid areas may be the impact of evaporation on the recharge process. In semi-arid and arid regions, average recharge rates estimated over large areas (40–374,000 km^2) range from 0.2 to 35 mm a^{-1}, representing 0.1 to 5% of long-term average annual precipitation [52]. Recent studies also demonstrated that the diffuse recharge beneath crops was 55–71 mm a^{-1} or 9–11% of the mean annual precipitation. These results were based on the chloride mass balance of soil profiles in Loess Plateau with precipitation ranging from 360 to 623 mm yr^{-1} [53]. Considerable soil water augmented by precipitation did not disappear due to evaporation [5,8,9,54]. The soil water being affected by evaporation remained in the vadose zone and finally recharged groundwater in such areas [55]. Thus, the resultant stable isotopic composition of the groundwater was depleted compared to the source water in the areas [5,10–12]. By contrast, in the hyper-arid area, the soil water that remained near the surface, replenished by low-intensity and high-intensity precipitation, disappeared completely due to evaporation (Figures 2b and 4a). However, 29% of the high-intensity precipitation (Figure 2c) rapidly infiltrated deep enough to avoid evaporation (Figures 2b and 3), and finally recharged the groundwater. Thus, stable isotopes of the groundwater were not depleted compared to those of high-intensity precipitation (Figure 6).

7. Conclusions

Empirical research on groundwater recharge in hyper-arid regions continues to be limited. Towards this end, this study contributes to the literature by demonstrating how high-intensity precipitation could induce groundwater recharge even in a hyper-arid region. This study has important implications for groundwater management and recharge modeling in the Chinese region and also globally in other regions which share similar hydrogeological and lithological characteristics.

Author Contributions: T.A., J.K., and M.N. conceived and designed the project; T.A. and J.K. performed the field survey; T.A., J.K., K.F., and M.N. analyzed the data; T.A. wrote the paper; J.K., K.F., M.N., M.T., R.A., and A.K. improved the paper.

Funding: Please add: This work was funded by the JSPS KAKENHI Grant Numbers 04J05742 and 17K12855.

Acknowledgments: The authors extend sincere thanks to T.H. and O.A. of Nagoya University and to the many local people who generously cooperated with us. This study was partly conducted with a contribution from the Oasis Project (Historical evolution of adaptability in an oasis region to water resource changes) promoted by the Research Institute for Humanity and Nature (RIHN).

Conflicts of Interest: The authors declare no conflict of interest.

References

1. United Nations Environment Program (UNEP). *World Atlas of Desertification*, 2nd ed.; Middleton, N., Thoma, D., Eds.; UNEP: London, UK, 1997.
2. Gee, G.W.; Wierenga, P.J.; Andraski, B.J.; Young, M.H.; Fayer, M.J.; Rockhold, M.L. Variations in water balance and recharge potential at three western desert sites. *Soil Sci. Soc. Am. J.* **1994**, *58*, 63–72. [CrossRef]
3. Wu, J.; Zhang, R. Analysis of rainfall-infiltration recharge to groundwater. Proceedings of Fourteenth Annual American Geophysical Union, Hydrology Days, Fort Collins, CO, USA, 5–8 April 1994; pp. 420–430.
4. Onodera, S. The mechanism of concentrated groundwater recharge in a tropical semiarid region. *J. Jpn. Assoc. Hydrol. Sci.* **1996**, *26*, 87–98.
5. Tsujimura, M.; Abe, Y.; Tanaka, T.; Shimada, J.; Higuchi, S.; Yamanaka, T.; Davaa, G.; Oyunbaatar, D. Stable isotopic and geochemical characteristics of groundwater in Kherlen River basin, a semi-arid region in eastern Mongolia. *J. Hydrol.* **2007**, *333*, 47–57. [CrossRef]
6. Carter, R.; Morgulis, E.; Dottridge, J. Groundwater modeling with limited data: A case study in a semi-arid dune field of northeast Nigeria. *Q. J. Eng. Geol.* **1994**, *27*, 85–94. [CrossRef]
7. Gao, Z.; Zhang, L.; Cheng, L.; Zhang, X.; Cowan, T.; Cai, W.; Brutsaert, W. Groundwater storage trends in the Loess Plateau of China estimated from streamflow records. *J. Hydrol.* **2015**, *530*, 281–290. [CrossRef]
8. Allison, G.B.; Hughes, M.W. The use of natural tracers as indicators of soil-water movement in a temperate semi-arid region. *J. Hydrol.* **1983**, *60*, 157–173. [CrossRef]
9. Barnes, C.J.; Allison, G.B. Tracing of water movement in the unsaturated zone using stable isotopes of hydrogen and oxygen. *J. Hydrol.* **1988**, *100*, 143–176. [CrossRef]
10. Magaritz, M.; Aravena, R.; Peña, H.; Suzuki, O.; Grilli, A. Water chemistry and isotope study of streams and springs in northern Chile. *J. Hydrol.* **1989**, *108*, 323–341. [CrossRef]
11. Sami, K. Recharge mechanisms and geochemical processes in a semi-arid sedimentary basin, Eastern Cape, South Africa. *J. Hydrol.* **1992**, *139*, 27–48. [CrossRef]
12. Navada, S.V.; Nair, A.R.; Rao, S.M.; Paliwall, B.L.; Doshi, C.S. Groundwater recharge studies in arid region of Jalore, Rajasthan using isotope techniques. *J. Arid Environ.* **1993**, *24*, 125–133. [CrossRef]
13. Huang, T.; Pang, Z. Estimating groundwater recharge following land-use change using chloride mass balance of soil profiles: A case study at Guyuan and Xifeng in the Loess Plateau of China. *Hydrogeol. J.* **2011**, *19*, 177–186. [CrossRef]
14. Edmunds, W.M.; Fellman, E.; Goni, I.B.; Prudhomme, C. Spatial and temporal distribution of groundwater recharge in northern Nigeria. *Hydrogeol. J.* **2002**, *10*, 205–215. [CrossRef]
15. Flint, A.; Flint, L.; Kwicklis, E.; Bodvarsson, G. Estimating recharge at Yucca Mountain, Nevada, USA: Comparison of methods. *Hydrogeol. J.* **2002**, *10*, 180–204. [CrossRef]
16. Foster, S. Quantification of groundwater recharge in arid regions: A practical view for resource development and management. In *Estimation of Natural Ground Water Recharge*; Simmers, I., Ed.; Reidel: Dordrecht, the Netherlands, 1988; pp. 323–338. ISBN 9027726329.
17. Lerner, D.N.; Issar, A.S.; Simmers, I. Groundwater Recharge: A Guide to Understanding and Estimating Natural Recharge. In *International Contributions to Hydrogeology IAH*; Verlag Heinz Heise: Hannover, Germany, 1990; Volume 8.
18. Li, Z.; Lin, X.; Coles, A.E.; Chen, X. Catchment-scale surface water-groundwater connectivity on China's Loess Plateau. *Catena* **2017**, *152*, 268–276. [CrossRef]

19. De Vries, J.J.; Simmers, I. Groundwater recharge: An overview of processes and challenges. *Hydrogeol. J.* **2002**, *10*, 5–17. [CrossRef]
20. Scanlon, B.R.; Healy, R.W.; Cook, P.G. Choosing appropriate techniques for quantifying groundwater recharge. *Hydrogeol. J.* **2002**, *10*, 18–39. [CrossRef]
21. Zhu, G.; Su, Y.; Huang, C.; Qi, F.; Liu, Z. Hydrogeochemical processes in the groundwater environment of Heihe River Basin, Northwest China. *Environ. Earth Sci.* **2010**, *60*, 139–153. [CrossRef]
22. Sakai, A.; Fujita, K.; Nakawo, M.; Yao, T. *Role of Glacier Runoff in the Heihe Basin*; Research Institute for Humanity and Nature: Kamigamo, Japan, 2005.
23. Akiyama, T.; Kharrazi, A.; Li, J.; Avtar, R. Agricultural water policy reforms in China: A representative look at Zhangye City, Gansu Province, China. *Environ. Monit. Assess.* **2018**, *190*. [CrossRef] [PubMed]
24. Ding, Y.; Li, Z. Tectonic characteristics of Yinen-Ejina Banner Basin reflected by aeromagnetic survey. *Geophys. Geochem. Explor.* **1999**, *23*, 191–194.
25. Wu, Y.; Chen, C.; Shi, S.; Li, Z. Three dimensional numerical simulation of groundwater system in Ejina Basin, Heihe River, Northwestern China. *J. China Univ. Geosci.* **2003**, *28*, 527–532.
26. Chao, B.; Gao, Q. *Grassland Type Map of the Heihe River Basin, China*; Institute of Desert Research Academia Sinica: Lanzhou, China, 1988.
27. Wang, G.; Cheng, G. Water resource development and its influence on the environment in arid areas of China—The case of the Hei River basin. *J. Arid Environ.* **1999**, *43*, 121–131.
28. Zha, J. A study of water resources evaluation in the north and northwest China. *Adv. Water Sci.* **1997**, *8*, 44–47.
29. Zhu, Y.; Wu, Y.; Drake, S. A survey: Obstacles and strategies for the development of ground-water resources in arid inland river basins of Western China. *J. Arid Environ.* **2004**, *59*, 351–367. [CrossRef]
30. Wen, X.; Wu, Y.; Su, J.; Zhang, Y.; Liu, F. Hydrochemical characteristics and salinity of groundwater in the Ejina Basin, Northwestern China. *Environ. Geol.* **2005**, *48*, 665–675. [CrossRef]
31. Akiyama, A.; Sakai, A.; Yamazaki, Y.; Wang, G.; Fujita, K.; Nakawo, M.; Kubota, J.; Konagaya, Y.T. Surfacewater-groundwater interaction in the Heihe River basin, Northwestern China. *Bull. Glaciol. Res.* **2007**, *24*, 87–94.
32. Webb, E.; Pearman, G.; Leuning, R. Correction of Flux Measurements for Density Effects due to Heat and Water Vapour Transfer. *Q. J. R. Meteorol. Soc.* **1980**, *106*, 85–100. [CrossRef]
33. Western, A.W.; Seyfried, M.S. A calibration and temperature correction procedure for the water-content reflectometer. *Hydrol. Process.* **2005**, *19*, 3785–3793. [CrossRef]
34. Monteith, J.L. Evaporation and surface temperature. *Q. J. R. Meteorol. Soc.* **1981**, *107*, 1–27. [CrossRef]
35. Kondo, J.; Saigusa, N.; Sato, T. A Parameterization of Evaporation from Bare Soil Surfaces. *J. Appl. Meteorol.* **1990**, *29*, 385–389. [CrossRef]
36. Saigusa, N. Heat balance at soil surfaces. In *Meteorology for Water Environment: Heat and Water Balances at Surfaces*; Kondo, J., Ed.; Asakura Publishing: Tokyo, Japan, 1994; pp. 185–205.
37. Ohta, T.; Hiyama, T.; Tanaka, H.; Kuwada, T.; Trofim, M.; Ohata, T.; Fukushima, Y. Seasonal variation in the energy and water exchanges above and below a larch forest in eastern Siberia. *Hydrol. Process.* **2001**, *15*, 1459–1476. [CrossRef]
38. Tamagawa, I. Turbulent characteristics and bulk transfer coefficients over the desert in the HEIFE area. *Bound. Layer Meteorol.* **1996**, *77*, 1–20. [CrossRef]
39. Peng, H.; Mayer, B.; Harris, S.; Roy Krouse, H. A 10-year record of stable isotope ratios of hydrogen and oxygen in precipitation at Calgary, Alberta, Canada. *Tellus B* **2004**, *56*, 147–159. [CrossRef]
40. Dansgaard, W. Stable isotopes in precipitation. *Tellus* **1964**, *16*, 436–468. [CrossRef]
41. Gibson, J.J.; Price, J.S.; Aravena, R.; Fitzgerald, D.F.; Maloney, D. Runoff generation in a hypermaritime bog-forest upland. *Hydrol. Process.* **2000**, *14*, 2711–2730. [CrossRef]
42. Ingraham, N.L. Isotopic variation in precipitation. In *Isotope Tracers in Catchment Hydrology*; Kendall, C., McDonnell, J., Eds.; Elsevier: New York, NY, USA, 1998; pp. 87–118.
43. Moreira, M.; Sternberg, L.; Martinelli, L.; Victoria, R.; Barbosa, E.; Bonates, L.; Nepstad, D. Contribution of transpiration to forest ambient vapour based on isotopic measurements. *Glob. Chang. Biol.* **1997**, *3*, 439–450. [CrossRef]

44. Craig, H.; Gordon, L. Deuterium and oxygen-18 variations in the ocean and the marine atmosphere. Proceedings of a Conference on Stable Isotopes in Oceanographic Studies and Paleotemperatures, Spoleto, Italy, 26–27 July 1965; Tongiorgi, E., Ed.; Lischi & Figli: Pisa, Italy, 1965; pp. 9–130.
45. Majoube, M. Fractionnement en Oxygène 18 et en Deutérium entre l'eau et sa vapeur. *J. Chim. Phys.* **1971**, *68*, 1423–1436. [CrossRef]
46. Sofer, Z.; Gat, J. The isotopic composition of evaporating brines: Effects of the isotopic ratio in saline solutions. *Earth Planet. Sci. Lett.* **1975**, *26*, 179–186. [CrossRef]
47. Merlivat, L. Molecular diffusivities of H216O, HD16O, and H218O in gases. *J. Chem. Phys.* **1978**, *69*, 2864. [CrossRef]
48. Flanagan, L.B.; Ehleringer, J.R. Stable isotope composition of stem and leaf water: Applications to the study of plant water use. *Funct. Ecol.* **1991**, *5*, 270–277. [CrossRef]
49. Wang, X.F.; Yakir, D. Using stable isotopes of water in evapotranspiration studies. *Hydrol. Process.* **2000**, *14*, 1407–1421. [CrossRef]
50. Craig, H. Isotopic Variations in Meteoric Waters. *Science* **1961**, *133*, 1702–1703. [CrossRef] [PubMed]
51. Kobayashi, T.; He, W.J.; Nagai, H. Mechanisms of evaporation from soil with a dry surface. *Hydrol. Process.* **1998**, *12*, 2185–2191. [CrossRef]
52. Scanlon, B.R.; Keese, K.E.; Flint, A.L.; Flint, L.E.; Gaye, C.B.; Edmunds, W.M.; Simmers, I. Global synthesis of groundwater recharge in semiarid and arid regions. *Hydrol. Process.* **2006**, *20*, 3335–3370. [CrossRef]
53. Huang, T.; Pang, Z.; Liu, J.; Ma, J.; Gates, J. Groundwater recharge mechanism in an integrated tableland of the Loess Plateau, northern China: Insights from environmental tracers. *Hydrogeol. J.* **2017**, *25*, 2049–2065. [CrossRef]
54. Tsujimura, M.; Tanaka, T. Evaluation of evaporation rate from forested soil surface using stable isotopic composition of soil water in a headwater basin. *Hydrol. Process.* **1998**, *12*, 2093–2103. [CrossRef]
55. Gat, J.R. Oxygen and hydrogen isotopes in the hydrologic cycle. *Annu. Rev. Earth Planet. Sci.* **1996**, *24*, 225–262. [CrossRef]